Catal Lett (2007) 119:265–270
DOI 10.1007/s10562-007-9228-0

Role of Surface Area in Oxygen Storage Capacity of Ceria–Zirconia as Soot Combustion Catalyst

Qing Liang · Xiaodong Wu · Xiaodi Wu · Duan Weng

Received: 11 September 2006 / Accepted: 20 July 2007 / Published online: 15 August 2007

Abstract Two thermal stable phases, $Ce_{0.75}Zr_{0.25}O_2$ and $Ce_{0.16}Zr_{0.84}O_2$, with different surface area were prepared by coprecipitation. The oxygen storage capacity (OSC) measurements were carried out at 500 °C under both transient (CO–O_2 cycle at 0.05, 0.1 and 0.25 Hz) and stationary reaction conditions (CO pulse). In the oxygen storage/release process, the rate-determine step is surface reactions when the specific surface area is lower than 60 m^2/g. When the surface area increases further, the influence of surface area is less important. The increased surface area favors diesel soot catalytic combustion via providing more redox sites to activate adsorbed oxygen. Nevertheless, this effect is less important when the specific surface area is larger than 40 m^2/g, especially under loose contact condition.

Keywords CeO_2–ZrO_2 · Specific surface area · OSC · Soot catalytic oxidation

1 Introduction

Ceria–zirconia mixed oxides have been widely used in automotive three-way catalysts (TWCs) for their good oxygen storage/release performance [1–4]. Recently it has been found that ceria and ceria–zirconia have a potential to increase the oxidation rate of soot because of the creation of "active oxygen" and high oxygen storage capacity (OSC) [5–10]. In the absence of catalyst, soot oxidation takes place above 500 °C. The creation of active oxygen species starts from 400 °C for CeO_2 and it will decrease the soot oxidation temperature [8]. Participation of lattice oxygen in soot oxidation may contribute to overall activity, especially in CeO_2–ZrO_2 and when surface area is low [9].

The relationship between the OSC of ceria–zirconia and its structural and textual properties has been investigated. Mamontov et al. [11] established a direct correlation between the concentration of vacancy-interstitial oxygen defects and OSC. Si et al. [12] found that the lattice strains in ceria–zirconia showed a linear relationship with their OSC values. Local structure around Ce and Zr was also believed to be a determining factor of the OSC of mixed oxides [13–15].

Specific surface area plays an important role in oxygen storage/release process for pure ceria since the OSC is attributed mainly to the release of surface oxygen [16, 17]. However, no consensus opinions have been achieved on the role of surface area in CeO_2–ZrO_2 mixed oxides. In some studies which measured the OSC in stationary mode, the surface area is not suggested to be a determining factor for total OSC [11, 16]. Suda et al. [16] presumed that the OSC of CeO_2–ZrO_2 mixed oxides with more than 60 mol% ZrO_2 was independent of specific surface area and the OSC was controlled by the thermodynamic equilibrium of the redox reaction of Ce ions. But other opinions also exit. Hori et al. [18] suggested that surface processes, rather than migration of oxygen in the bulk, were limiting the reduction process rate according to CO pulse measurement. In this work, different modes of OSC measurement were taken to investigate the role of surface area in oxygen storage/release processes.

It has been confirmed that no phase de-mixing occurs and there is still a very good agreement between surface and bulk compositions for $Ce_{0.16}Zr_{0.84}O_2$ and

Q. Liang · X. Wu (✉) · X. Wu · D. Weng
Laboratory of Advanced Materials, Department of Materials Science and Engineering, Tsinghua University, Beijing 100084, China
e-mail: wuxiaodong@tsinghua.edu.cn

$Ce_{0.75}Zr_{0.25}O_2$ even after ageing at 1,000 °C [19]. Thus, these two compositions were chosen in this paper to abate phase deviation and keep compositional heterogeneity as much as possible. In the soot catalytic oxidation process, the surface area of the catalyst plays a crucial role because it is closely related to the gas-catalyst interactions as well as OSC. So the soot oxidation tests were also performed.

2 Experimental

2.1 Catalyst Preparation

CeO_2–ZrO_2 mixed oxides were prepared by coprecipitation in an aqueous solution containing excess NH_4OH, starting from a solution of $Ce(NH_4)_2(NO_3)_6$ and $ZrO(NO_3)_2$ according to the required proportion. The precipitate was filtered, washed several times with deionized water, and then dried at 110 °C for 24 h. The powders were calcined at 500, 700, 900 or 1,050 °C under flowing air for 2 h respectively to achieve different surface area. For brevity, the Ce-rich samples $Ce_{0.75}Zr_{0.25}O_2$ were referred to as CRX, while the Zr-rich samples $Ce_{0.16}Zr_{0.84}O_2$ were referred to as ZRX, where X = 5, 7, 9, K represented the calcination temperature of 500, 700, 900 or 1,050 °C, respectively. Two high-surface-area samples were prepared by a novel coprecipitation method with adding surfactant of cetyltrimethylammonium bromide into the precursor solution, and were named as CRS and ZRS, respectively after calcination at 500 °C.

2.2 Catalyst Characterization

The powder X-ray diffraction (XRD) experiments were performed on a Japan Science D/max-RB diffractometer employing Cu Kα radiation (λ = 1.5418 Å). The X-ray tube was operated at 40 kV and 120 mA. The X-ray powder diffractogram was recorded at 0.02° intervals in the range of $20° \leq 2\theta \leq 80°$ with a scanning velocity of 6°/min.

The specific surface areas of the samples were measured using the N_2 adsorption isotherm at −196 °C by the one-point Brunauer–Emmett–Teller (BET) method using an automatic surface analyzer (Quantachrome NOVA instrument). The samples were degassed in flowing N_2 at 200 °C for 2 h.

2.3 OSC Measurement

Two forms of OSC measurements were carried out, including CO–O_2 cycle and CO pulse measurements. The measurements were carried out in a flow reactor system, designed for powder samples, equipped with solenoid valves for rapid introduction of 4% CO/He or 2% O_2/He pulses. Typically 25 mg powders were loaded into a 1.0 cm i.d. quartz tube reactor and a total gas flow rate of 300 cm^3/min was employed. 1% Ar was injected along with He as an internal standard for quantification of gas concentrations. The signals of the outlet gas were detected by an on-line quadrupole mass spectrometer (Omnistar 200).

For CO–O_2 cycle measurements at 500 °C, alternate 4% CO/He (2, 5 or 10 s) and 2% O_2/He (2, 5 or 10 s) pulses were injected on the catalyst at a frequency of 0.25, 0.1 or 0.05 Hz. The dynamic OSC was quantified in terms of micromoles of CO_2 produced per gram of catalyst (μmol O_2/g cat.) by calculating integrated amounts of CO_2 produced during every single CO–O_2 cycle.

Prior to CO pulse measurements, the sample was first heated in 2% O_2/He at 500 °C for at least 20 min. The sample was further purged in pure He for 30 min to remove oxygen from the system and then exposed to 4% CO/He (5 s) and He (40s) pulse at 500 °C. The total production of CO_2 per gram of catalyst in the first ten CO pulses was calculated, and was suggested to give the information of total OSC.

2.4 Soot Oxidation Test

Printex-U (Degussa) was used a model soot. Its particle size was 25 nm and specific surface was 100 m^2/g. The catalytic activity was evaluated by a temperature-programmed oxidation (TPO) reaction apparatus. Before the reaction, the soot-catalyst mixture, in a 1/10 weight ratio, were milled in an agate mortar for "tight contact" or mixed carefully with a spatula for "loose contact". 110 mg catalyst-soot mixture was placed in the tubular quartz reactor (i.d. = 10 mm), and the oxidation was carried out in the temperature range from 200 to 700 °C at a heating rate of 10 °C/min. The gas mixture composition was 10% O_2 in nitrogen with a flow rate of 500 ml/min. The concentrations of CO_2 and CO were determined on-line by a five-component analyzer FGA4015 with infrared sensor. Considering the formation of CO as a byproduct of soot oxidation (<5%), only the maximum rate temperature (T_m) for CO_2 produced in TPO curves was calculated.

3 Results and Discussion

3.1 Structural and Textural Properties

The X-ray diffraction patterns of the samples are shown in Fig. 1. For CRX series, all the peaks are consistent with the

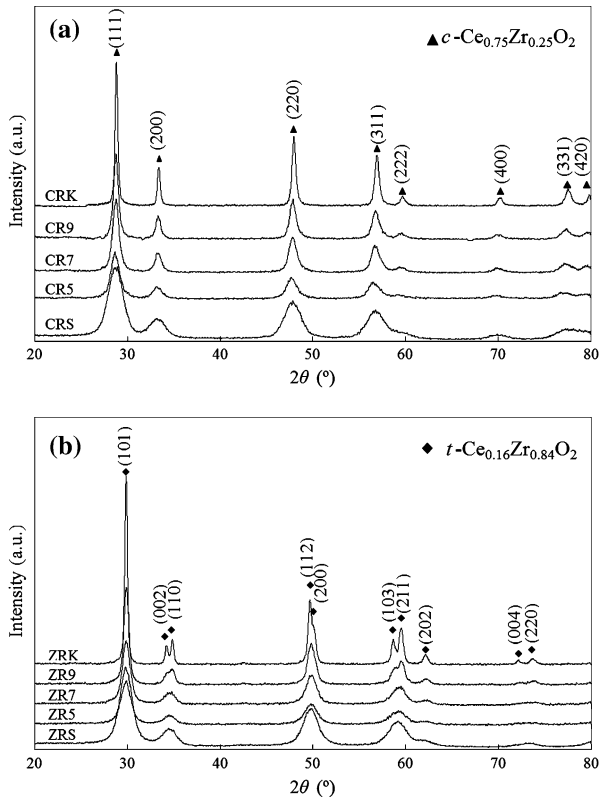

Fig. 1 X-ray diffraction patterns of (**a**) CRX and (**b**) ZRX series

characteristic peaks of a fluorite-like cubic phase referred to as $Ce_{0.75}Zr_{0.25}O_2$ (JCPDS card 28-0271). The peaks of ZRX series correspond well with a tetragonal phase referred to as $Ce_{0.16}Zr_{0.84}O_2$ (JCPDS card 38-1437). No phase segregation is detected under the calcination conditions here employed (500–1,050 °C).

Table 1 summarizes the structural and textural information of the samples. The surface area decreases rapidly with the increase of calcination temperature, while the Zr-rich sample shows a better thermal stability than the Ce-rich sample. The cell volume expands as the crystallite size decreases for both c-$Ce_{0.75}Zr_{0.25}O_2$ and t-$Ce_{0.16}Zr_{0.84}O_2$ except CRS and ZRS synthesized by different method. The most possible factor may be attributed to the generation of oxygen vacancies in the nanocrystalline materials, i.e. the formation of reduced Ce^{3+} species with larger ionic radius [20].

3.2 Effect of Surface Area on OSC

The total OSC values of the samples are shown in Fig. 2 as functions of specific surface area. Generally, the total OSC increases with increment of the surface area, but a parabolic curve rather than a linear relationship is obtained here. Total OSC is always thought to depend principally on the amount of Ce in the mixed oxides, and the surface area has less effect [21]. Since the Ce and Zr elements are suggested to be distributed homogeneously in the bulk and on the surface for these two series here, surface area becomes to be an important factor especially for the low-surface-area samples (<60 m^2/g). This effect is more obvious in the case of CRX series since there are much more Ce species provided by the mixed oxides. It is suggested that the surface structure is generally looser than the bulk structure and is less constrained to release oxygen atoms [16]. The higher the surface area is, the easier active oxygen could be released.

To further describe this effect, the dynamic OSC measurements, which are related to the most readily available oxygen atoms, were applied to evaluate the oxygen storage/release rate by dividing the dynamic OSC value by time scale. The production of CO_2 during the CO pulse passes through the formation of "weakly bond carbonates" that instantaneously decompose at 500 °C. Some more stable carbonates on reduced ceria are released during the O_2 pulse. Both parts of CO_2 evolution were considered in

Table 1 Structural and textural properties of the samples

Samples	BET surface area (m^2/g)	Lattice parameter[a] (Å)	Cell volume (Å^3)	Crystallite size[b] (Å)
CRS	147.71	5.390	156.59	41
CR5	74.67	5.391	156.68	67
CR7	39.04	5.386	156.24	91
CR9	22.7	5.383	155.98	113
CRK	8.15	5.364	154.34	208
ZRS	137.12	$a = b = 3.654$, $c = 5.221$	69.71	51
ZR5	90.37	$a = b = 3.652$, $c = 5.213$	69.53	48
ZR7	55.81	a = b = 3.646, $c = 5.223$	69.43	62
ZR9	34.71	$a = b = 3.643$, $c = 5.227$	69.37	112
ZRK	14.73	$a = b = 3.638$, $c = 5.234$	69.27	182

[a] Calculated from Rietveld refinement

[b] Calculated from XRD peak of (311) crystal plane using the Scherrer equation

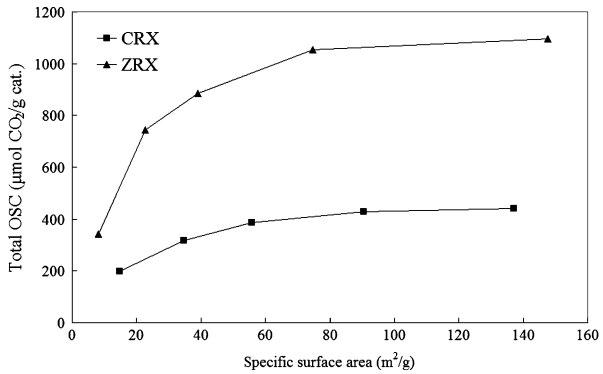

Fig. 2 Relationship between total OSC and specific surface area

this case since soot oxidation also involves oxygen from the support and gas-phase and the formation and decomposition of carbonates [22]. The results are shown in Fig. 3. When the BET surface area is lower than 60 m^2/g, a simple linear relationship between the rate of oxygen release and surface area is observed on both CRX and ZRX series. When the surface area further increases, a platform appears. This phenomenon exists under all three frequencies.

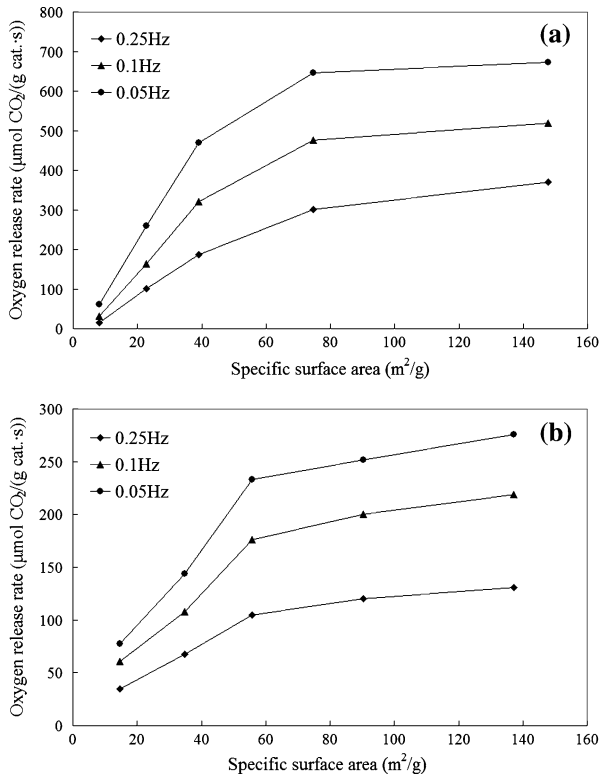

Fig. 3 Oxygen release rate under different frequencies on (**a**) CRX and (**b**) ZRX series

The following equilibrium describes the reduction of Ce^{4+} to Ce^{3+} in ceria–zirconia via the creation of oxygen vacancies.

$$2Ce_{Ce}^{x} + O_{O}^{x} \leftrightarrow V_{O}^{\cdot\cdot} + 2Ce_{Ce}^{'} + \frac{1}{2}O_2 \quad (1)$$

This reaction can be broken down into two steps: (i) formation of surface vacancies; (ii) migration of oxygen vacancies into the bulk. The rate-determining step can be either of these two parts [23]. If vacancy diffusion controls OSC, the influence of surface area would be expected to decrease. As shown in Fig. 3, different relationships between dynamic OSC and surface area imply different mechanisms for the high-surface-area and low-surface-area samples, respectively.

As shown in Table 2, the theoretical total amount of available surface oxygen per gram of catalyst is introduced based on an ideal but reasonable model [24]. If we compare it with the CO_2 produced in the first CO pulse under stationary reaction condition, it is seen that surface oxygen is totally depleted within the first pulse for all the samples except CRS. So part of bulk oxygen diffuses onto the surface and contributes to the CO_2 production in the first pulse. In this case, the average rate of oxygen release calculated from the second CO pulse seems to be a plausible indicator to reveal the oxygen mobility in the bulk. The calculated values for CRS, CR5 and CR7 are similar to each other, while those for CR9 and CRK decrease evidently. The oxygen diffusion coefficient expressed by $D = \frac{f\sigma_i kT}{C_i(Ze)^2}$[23] is assumed to be mainly influenced by the reaction temperature and the composition, where f is a correlation factor correlated with the crystal structure, σ_i is the ionic contribution to conductivity, k is the Boltzmann constant, T is the temperature, C_i is the concentration of charge carriers, and Ze their charge. It is confirmed by the work of Chiodelli [25] and Boaro [26] that the diffusion coefficient of oxygen is of the same order of magnitude in both nanocrystalline and bulk ceria–zirconia oxides with the ceria ratio of 0.75–0.8. Thus, the decrease of average oxygen release rate for CR9 and CRK can not be ascribed to the decrease of oxygen diffusion coefficient. This reveals that the rate-determine step would be surface reaction when the BET surface area is lower than 60 m^2/g. A similar phenomenon is observed on ZRX series that the average oxygen release rate decrease abruptly when the BET surface area is lower than 50 m^2/g. However, a similar conclusion can not be obtained since we are not sure whether the diffusion coefficients of oxygen are of the same order in low and high surface area zirconia-rich mixed oxides. These data are consistent with the previous studies which indicated when the BET surface area is higher than 50–60 m^2/g, its contribution to reducibility would be constant [27].

Table 2 The OSC performances of the samples

Samples	Theoretical available surface oxygen (μmol [O]/g cat.)[a]	CO_2 production in 1st CO pulse (μmol CO_2/g cat.)	CO_2 production in 2nd CO pulse (μmol CO_2/g cat.)	Average oxygen release rate (μmol [O]/(g cat. s)[b]
CRS	516	491	165	27.8[c]
CR5	260	395	137	27.4
CR7	136	316	131	26.2
CR9	79	169	106	21.2
CRK	29	29	32	6.4
ZRS	130	204	61	12.3
ZR5	86	151	59	11.8
ZR7	53	147	59	11.8
ZR9	33	93	35	7.1
ZRK	14	43	18	3.6

[a] Calculation method was presented in [23]

[b] Obtained by dividing the CO_2 produced in 2nd CO pulse by the time scale 5s

[c] For CRS, since the surface oxygen had not been totally consumed during the 1st CO pulse, the left surface oxygen was subtracted from the CO_2 production in the 2nd CO pulse when calculating the oxygen release rate

3.3 Relationship Between Surface Area and Soot Oxidation

Active oxygen plays an important role in soot catalytic oxidation when using ceria-based oxides as catalyst [8, 9, 28, 29], since the rate of active oxygen reacting with soot has been proved to be much faster than the rate of its combustion by gas-phase O_2. A typical mechanism to create active oxygen is the redox mechanism, which is gas oxygen activated on the partial reductive catalyst surface [9]. Thus the surface area is a critical factor in soot catalytic combustion since more redox sites of Ce^{4+}/Ce^{3+} locate on high-surface-area catalyst.

The relationship between T_m and surface area under different contact conditions are shown in Fig. 4. It is noticed that the influence of the surface area is less remarkable under loose contact condition than tight contact condition. Although there are more redox sites to create active oxygen on the high-surface-area samples, it is difficult for active oxygen to transfer from catalyst to soot particles under loose contact conditions. So a strong dependence of catalytic activity for soot oxidation against surface area is observed on the low-surface-area (<40 m^2/g) samples, which is also observed on thermal treated La-doped CeO_2 (<25 m^2/g) [29]. Tight contact condition brings more contact probability for soot and catalyst surface and access of gas phase oxygen is limited by geometrical factors, so active oxygen on the surface can participate in the reaction more easily and the influence of surface area is more remarkable. Nevertheless, the activity in soot combustion is less influenced by the surface area of the catalyst in the range of larger surface area (>40 m^2/g), which is consistent with the results on Fe-modified ceria

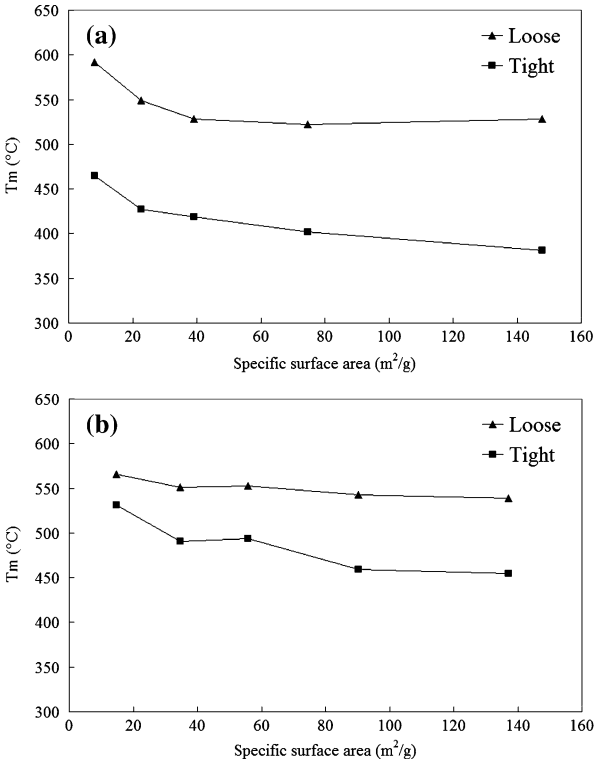

Fig. 4 Relationship between T_m and specific surface area over (**a**) CRX and (**b**) ZRX series

[10]. It is also easy to find that the catalytic activity of CRX is similar to that of ZRX under loose contact condition, but it is remarkable better under tight contact condition, which can be explained by this reason as well. It it notable that a more detailed study was recently carried out by Makkee et al. [30]. They pointed out that the meso/micro pore

volume and external surface area were more important parameters for the soot oxidation with O_2.

4 Conclusions

The influence of surface area on the OSC of ceria–zirconia can not be neglected. In the both stationary and dynamic oxygen storage/release processes, the rate-determine step would be surface reaction when the specific surface area is lower than 60 m^2/g, and this effect is less important when the specific surface area further increases. The surface area is not the only factor affecting the activity of ceria–zirconia for soot catalytic combustion. Although the high-surface-area samples provide more active oxygen, tight contact condition is also critical to provide more contact probability for active oxygen to transfer from catalyst to soot particles.

Acknowledgments The authors would like to acknowledge the Ministry of Science and Technology, PR China for the financial support of Project 2004CB719503 and National Natural Science Foundation of China for the financial support of Project 50502023.

References

1. Yao HC, Yu Yao YF (1984) J Catal 86:254
2. Kašpar J, Fornasiero P, Graziani M (1999) Catal Today 50:285
3. Sugiura M,Ozawa M, Suda A, Suzuki T, Kanazawa T (2005) Bull Chem Soc Jpn 78:752
4. Fornasiero P, Balducci G, Di Monte R, Kašpar J, Sergo V, Gubitosa G, Ferrero A, Graziani M (1996) J Catal 164:173
5. Harrison PG, Ball IK, Daniell W, Lukinskas P, Céspedes M, Miró EE, Ulla MA (2003) Chem Eng J 95:47
6. Zhu L, Wang X, Hao Z (2004) J Rare Earth 22:84
7. Tikhomirov K, Kröcher O, Elsener M, Wokaun A (2006) Appl-Catal B 64:72
8. Bueno-López A, Krishna K, Makkee M, Moulijn JA (2005) Catal Lett 99:203
9. Aneggi E, Boaro M, de Leitenburg C, Dolcetti G, Trovarelli A (2006) Catal Today 112:94
10. Aneggi E, de Leitenburg C, Dolcetti G, Trovarelli A (2006) Catal Today 114:40
11. Mamontov E, Egami T (2000) J Phys Chem B 104:11110
12. Si R, Zhang Y, Li S, Lin B, Yan C (2004) J Phys Chem B 108:12481
13. Mamontov E, Brezny R, Koranne M, Egami T (2003) J Phys Chem B 107:13007
14. Nagai Y, Yamamoto T, Tanaka T, Yoshida S, Nonaka T, Okamoto T, Suda A, Sugiura M (2001) J Synchrotron Rad 8:616
15. Nagai Y, Yamamoto T, Tanaka T, Yoshida S, Nonaka T, Okamoto T, Suda A (2002) Catal Today 74:225
16. Suda A, Yamamura K, Ukyo Y, Sasaki T, Sobukawa H, Tanabe T, Nagai Y, Sugiura M (2004) J Ceram Soc Jpn 112:581
17. Trovarelli A (1996) Catal Rev Sci Eng 38:439
18. Horia CE, Permana H, Simon Ng KY, Brenner A, More K, Rahmoeller KM, Belton D (1998) ApplCatal B 16:105
19. Bozo C, Gaillard F, Guilhaume Nolven (2001) Appl Catal A 220:69
20. Di Monte R, Krašpa J (2005) J Mater Chem 15:633
21. Sugiura M (2003) Catal Surv Asia 7:77
22. Aneggi E, Boaro M, de Leitenburg C, Dolcetti G, Trovarelli A (2006) J Alloy Compd 408–412:1101
23. Boaro M, de Leitenburg C, Dolcetti G, Trovarelli A (2000) J Catal 193:338
24. Madier Y, Descorme C, Le Govic AM, Duprez D (1999) J Phys Chem B 103:10999
25. Chiodelli G, Flor G, Scagliotti M (1996) Solid State Ionics 91:109
26. Boaro M, Trovarelli A, Hwang J, Mason TO (2002) Solid State Ionics 147:85
27. Giordano F, Trovarelli A, de Leitenburg C, Giona M (2000) J Catal 193:273
28. Setiabudi A, Chen J, Mul G, Makkee Mi, Moulijn JA (2004) Appl Catal B 51:9
29. Bueno-López A, Krishna K, Makkee M, Moulijn JA (2005) J Catal 230:237
30. Krishna K, Bueno- López A, Makkee M, Moulijn JA (2007) Appl Catal B 75:191